Chapter

Rectenna Systems for RF Energy Harvesting and Wireless Power Transfer

Mohamed Aboualalaa and Hala Elsadek

Abstract

With the rapid development of the wireless systems and demands of low-power integrated electronic circuits, various research trends have tended to study the feasibility of powering these circuits by harvesting free energy from ambient electromagnetic space or by using dedicated RF source. Wireless power transmission (WPT) technology was first pursued by Tesla over a century ago. However, it faced several challenges for deployment in real applications. Recently, energy harvesting and WPT technologies have received much attention as a clean and renewable power source. Rectenna (rectifying antenna) system can be used for remotely charging batteries in several sensor networks at internet of things (IoT) applications as commonly used in smart buildings, implanted medical devices and automotive applications. Rectenna, which is used to convert from RF energy to usable DC electrical energy, is mainly a combination between a receiving antenna and a rectifier circuit. This chapter will present several designs for single and multiband rectennas with different characteristics for energy harvesting applications. Single and multiband antennas as well as rectifier circuits with matching networks are introduced for complete successful rectenna circuit models. At the end of the chapter, a dual-band rectenna example is introduced with a detailed description for each section of the rectenna.

Keywords: dedicated RF source, directive radiation pattern, high gain antenna, rectenna (rectifying antenna), RF energy harvesting, wireless power transmission (WPT)

1. Introduction

Wireless power transmission (WPT) can be categorized into three different categories as depicted in **Figure 1**: near-field inductive or resonant coupling, far-field directive powering, and far-field ambient wireless energy harvesting. For the first category, it usually takes place between two coils, one is the primary and the other is the secondary. The main goal is to transfer the power from the primary coil to the secondary coil for several of centimeter as a separation distance between them [1–3]. Many defected ground structure (DGS)-based designs are proposed for this type of the wireless power transfer [4–6] to give a high efficiency coupled system.

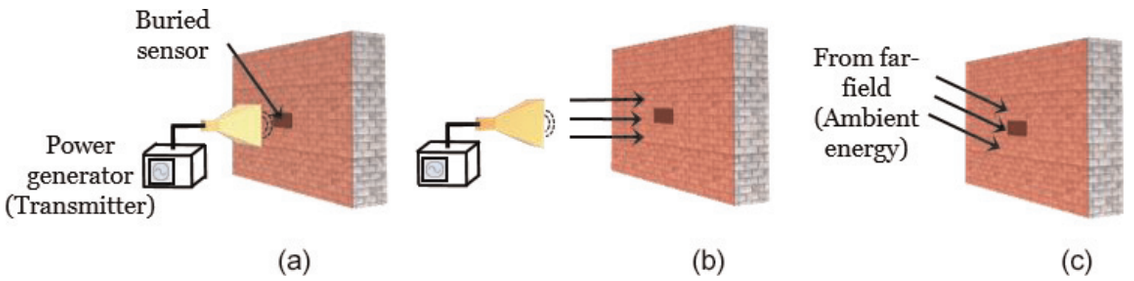

Figure 1.
WPT categories (a) near-field inductive or resonant coupling, (b) far-field directive powering and (c) far-field ambient wireless energy harvesting.

The second category of WPT is far-field directive powering that is used with directive power transmission which means the transmission occurs in the far-field zone but with well-defined direction of the source. This sort of WPT is useful for solar power satellites (SPS) applications [7–9] or with intentional powering such as using a dedicating source with well-known direction to power a network of wireless sensors, each sensor has built-in rectenna which is used as a renewable power source to power the connected sensor. The third type is far-field energy harvesting. The receiver does not know the direction of the received power. So, one of the main goals in this type is how to increase the probability of reception by designing antennas with wide beam-width and multiple or wideband resonance frequencies.

Near-field WPT offers a solution to short range powering for electronic devices, it becomes widely commercialized for several wireless applications [10–12]. Near-field transmission can also be useful with wireless implantable devices [13–15]. Nevertheless, near-field WPT suffers from severe issue with regard to the transmitting distance, it covers only very short range distances (few centimeters); therefore this limits its applications. On the other hand, the powering scheme of far-field dedicated source or free ambient powering technique can overcome this problem because of the long-distance charging capability. Several studies are introduced in wireless energy harvesting [16–25]. Although, the great focusing on the wireless energy harvesting, there are many obstacles in the way of free source energy harvesting. One of the main issues is that low input power levels of the ambient energy. Consequently, there are many research papers introduced for rectennas at low input power levels. However, single band rectennas have a simple structures, many research studies [26–31] have investigated the multi-band rectennas as a trial for increasing the scavenging received power with the same rectenna device; various single and multi-band rectennas are presented. Also, there are big challenges with respect to working the rectenna with fixed conversion efficiency values over a wide range of the received signal. Thus, Section 2 introduces a literature survey about single and multiband frequency operation of different rectennas; also, various rectennas' designs working at low input power and over wide input power range are discussed. Finally, in Section 3, dual-band rectenna using voltage doubler rectifier and four-section matching network is discussed as an example for a dual-band operation to illustrate the different stages of the whole rectenna system elaborately. The dual-band antenna, firstly, is designed, fabricated and measured separately to check the antenna performance. Then, the rectifier and the matching network between the antenna and the rectifying circuit are also designed and tested independently. After that the integration between the antenna and rectifier is done on the same PCB substrate.

2. Literature review on rectennas

2.1 Low input received power rectennas

In [32], a compact dual-band rectenna is proposed as depicted in **Figure 2**. The rectenna has a conversion efficiency of 37 and 30% at 915 MHz and at 2.45 GHz,

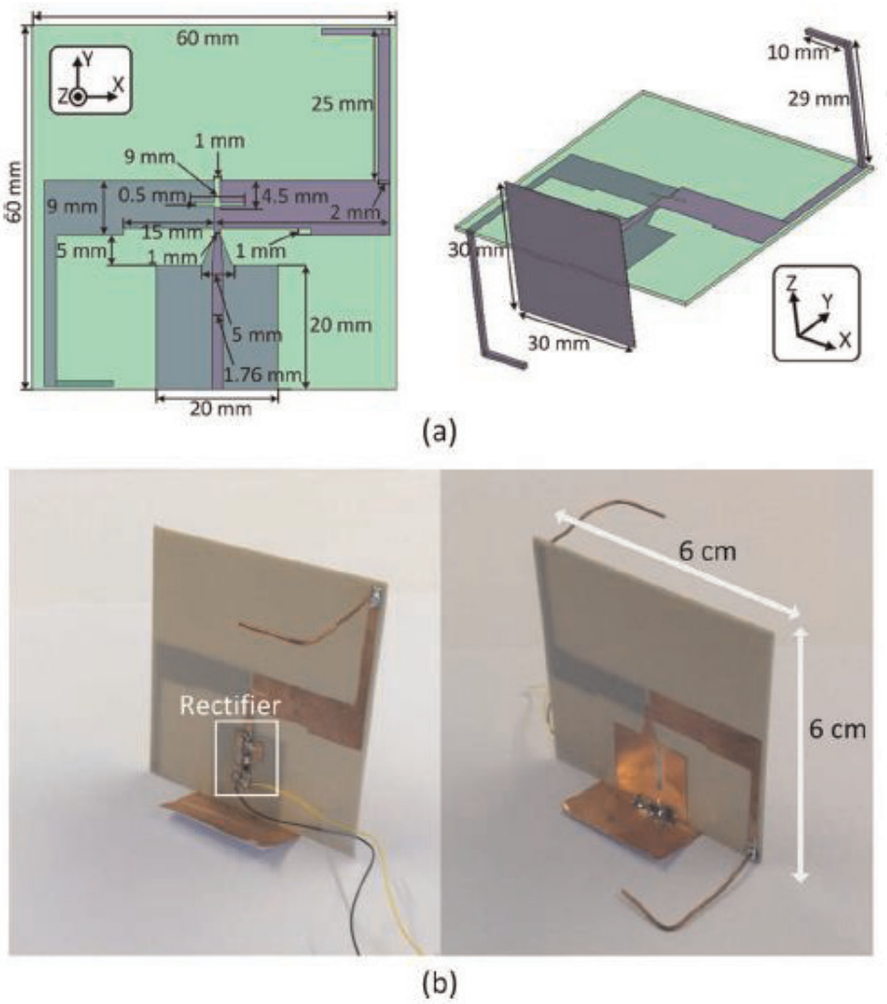

Figure 2.
Rectenna design: (a) design of the top and side view and (b) fabricated rectenna prototype [32].

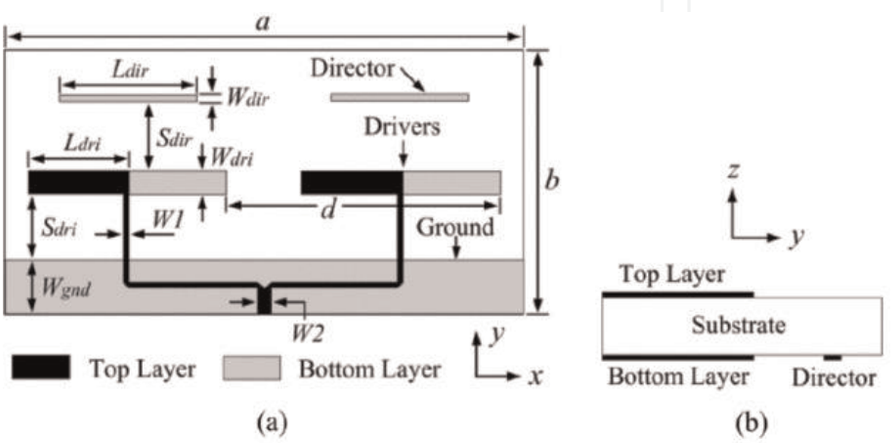

Figure 3.
Layout of the quasi-Yagi subarray. (a) Top view. (b) Side view [33].

respectively, at input power of −9 dBm with resistive load of 2.2 kΩ. A dual-band rectenna using Yagi antenna for low input power applications shown in **Figure 3** is introduced in [33]. The rectenna offers an acceptable values for the conversion efficiencies, it reaches up to 34% at 1.84 GHz and 30% at 2.14 GHz for input power level of −20 dBm. A combination between the solar energy and RF energy harvesting is discussed in [34]. This solar rectenna, displayed in **Figure 4**, achieves RF-DC conversion efficiency of 15% with input power of −20 dBm at 850 MHz and 2.45 GHz. In [35], a 130 nm CMOS rectifier is proposed for ultra-low input power. **Figure 5** shows the rectenna structure. It consists of 10 stages to give the maximum efficiency of 42.8% at −16 dBm input power and output DC voltage of 2.32 V at

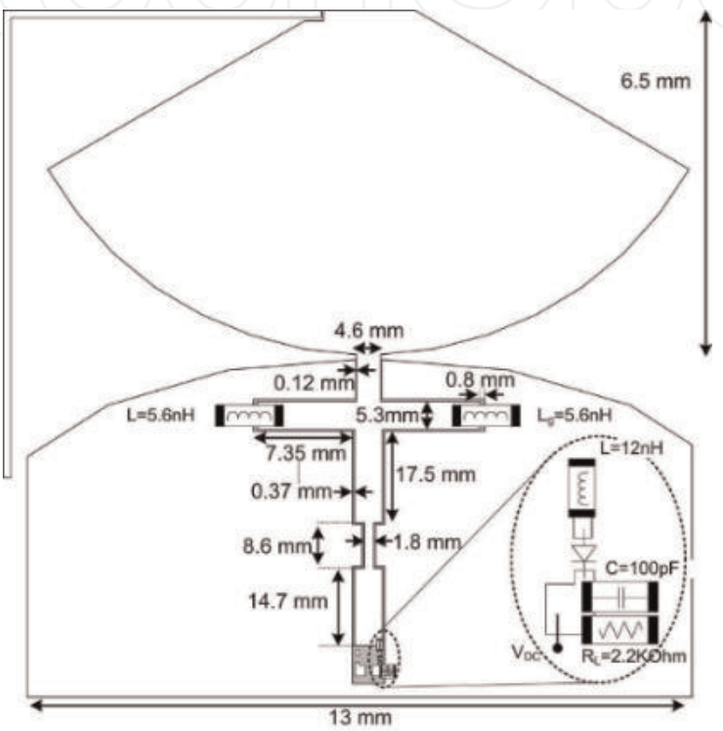

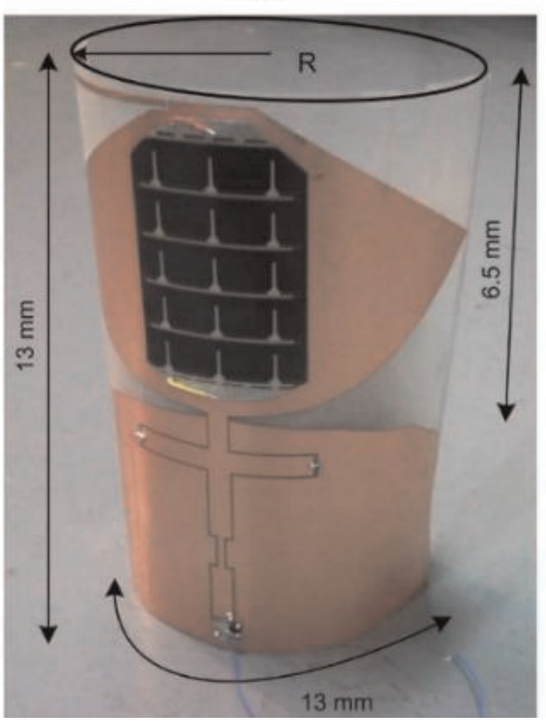

Figure 4.
Hybrid solar/EM rectenna [34].

DOI: http://dx.doi.org/10.5772/intechopen.89674

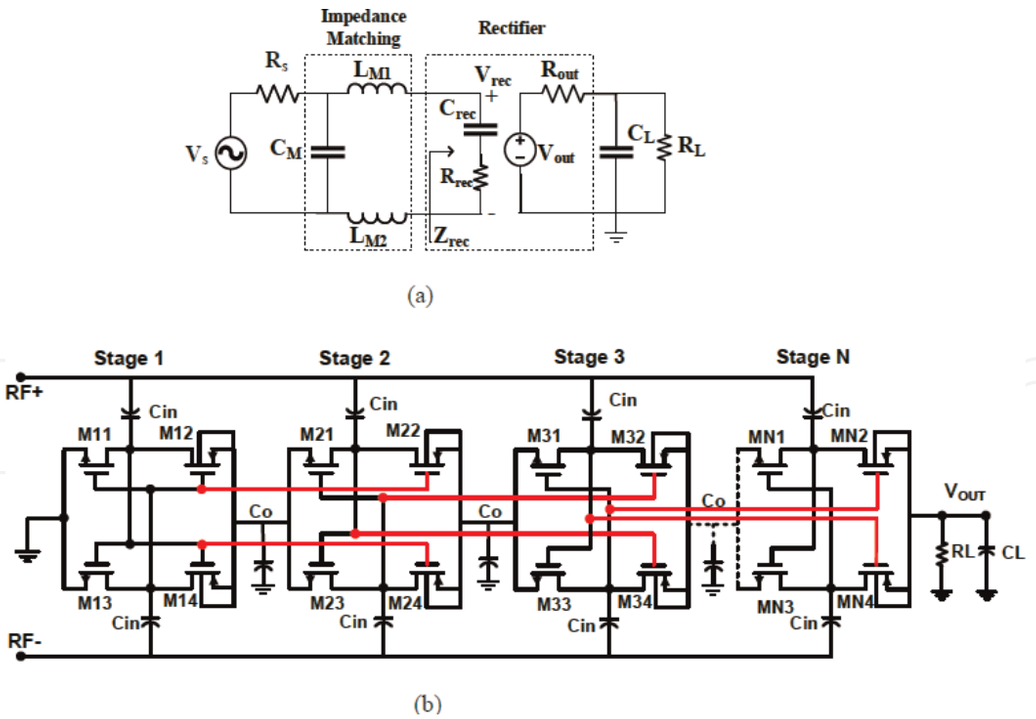

Figure 5.
(a) Proposed RF rectenna equivalent circuit, (b) self-compensated rectifier [35].

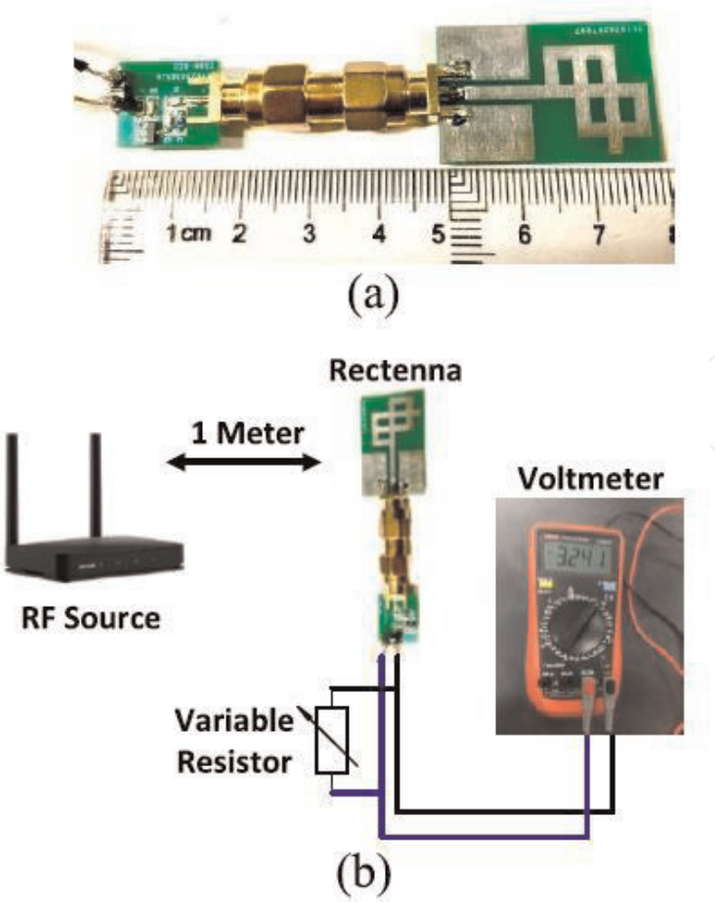

Figure 6.
(a) Complete prototype of the rectenna, (b) measurement set-up for rectenna system [16].

resistive load of 0.5 MΩ. A compact co-planar waveguide-fed rectenna using single stage Cockcroft Walton rectifier and L-shaped impedance matching network, shown in **Figure 6**, is presented in [16]. The RF-DC conversion efficiency is 68% with a received input signal power of 5 dBm at 2.45 GHz. This rectenna also gives conversion efficiencies around 48 and 19% at −10 and −20 dBm, respectively.

2.2 Single and multi-band rectennas

The simplest way in energy harvesting is to harvest from single frequency band; this in turn makes the design of matching circuit, which is used for maximum power transmission between the receiving antenna part and the rectifying circuit, is a little bit easier. In [36], a pentagonal antenna is used with series connection single diode to produce a single band rectenna at 5 GHz. The rectenna has maximum conversion efficiency of 46% at resistive load of 2 kΩ. In [37], a 3 × 2 rectangular patch array with a gain of 10.3 dBi is used with three-stage Dickson charge pump circuit for energy harvesting. The rectenna works at 915 MHz. **Figure 7** shows the antenna array as well as the rectifying circuit. The maximum rectifier efficiency is 41% at input power of 10 dBm. A semicircular slot antenna was presented for X-band planar rectenna (at 9.3 GHz) as depicted in **Figure 8** [38]. The rectenna gives RF-to-DC conversion efficiency of about 21% at an input power density of 245 μW/cm^2. 35 GHz rectenna using 4 × 4 patch antenna array, displayed in **Figure 9**, is proposed in [39]. The maximum RF-to-dc conversion efficiency is 67% with input RF received power of 7 mW.

Due to the variety in transmission bands for different wireless systems, there is a large ambient wasted energy at different frequencies. Consequently, the demand for harvesting from different bands increases. In [40], triple-band implanted rectenna is discussed. It works at 402 MHz, 433 MHz and 2.45 GHz with antenna has a stacked and spiral structure. **Figure 10** shows the antenna structure in addition to the rectifier design. It gives a conversion efficiency of 86% at input power of 11 dBm with 5 kΩ load resistor. A compact reconfigurable rectifying antenna has been presented in [41] for dual-band rectification at 5.2 and 5.8 GHz. The measured maximum conversion efficiencies of the proposed rectenna are 65.2 and 64.8% at 4.9 and 5.9 GHz, respectively, with 15 dBm input power. The rectenna fabricated prototype is shown in **Figure 11**. A dual frequency band rectenna has been developed in [42]. A planar inverted F-antenna is used with a voltage doubler circuit to configure a dual band rectenna.

With increasing the number of frequencies at which rectenna can harvest, the complexity of the matching circuit and the size of the rectenna increase. Therefore,

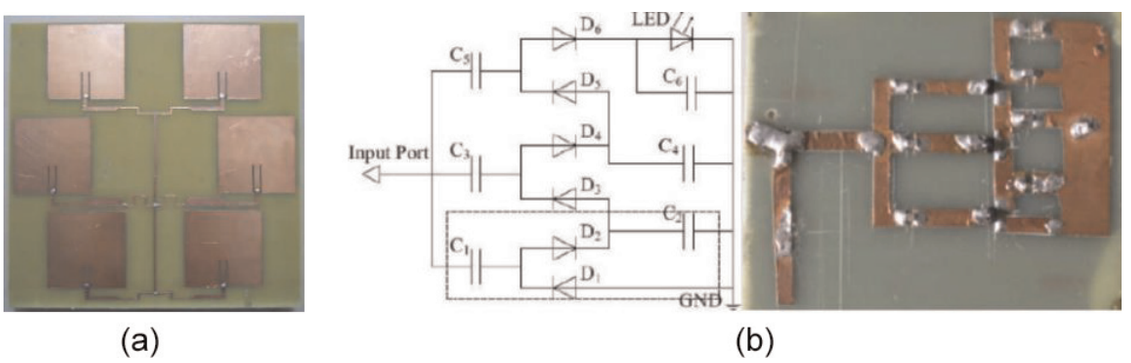

Figure 7.
Six elements antenna array (a) fabricated patch antenna array, (b) fabricated rectifier [37].

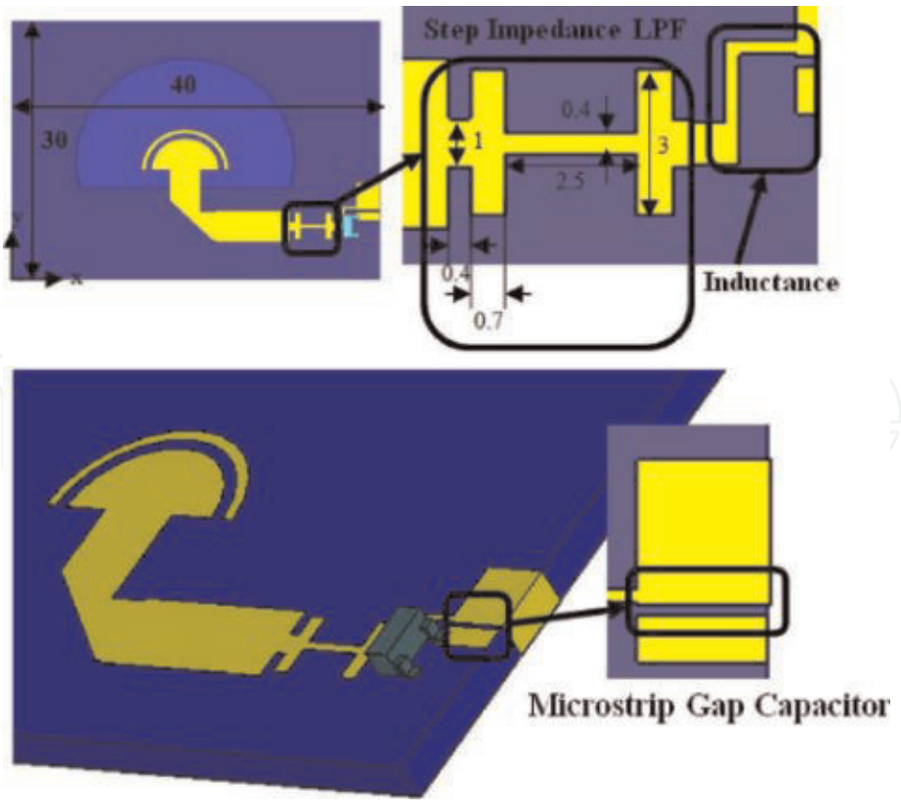

Figure 8.
Geometry of the X-band rectenna [38].

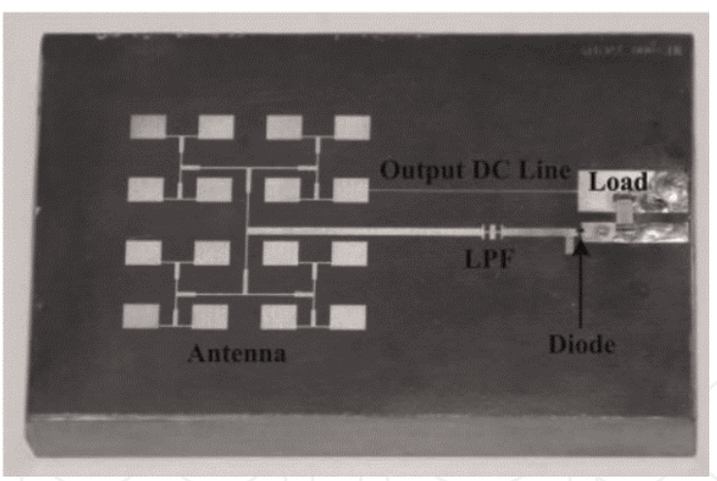

Figure 9.
Fabricated rectenna [39].

dual-band is the best choice in the designing of rectenna systems because it combines between the simplicity and the scavenging from more than one frequency band.

2.3 Wide input received power rectennas

There are several studies that are proposed to guarantee stable fixed RF-DC conversion efficiency over a wide band of the input power. In [43], dual-band rectifier with extended input power range is proposed. The rectifier schematic circuit and the fabricated design is displayed in **Figure 12**. The rectifier offers above 30% conversion efficiency with input power range from −15 to 20 dBm and the

maximum value is 60% from 5 to 15 dBm. Impedance compression network (ICN) techniques is discussed in [44] to fix RF-dc conversion efficiency over a wide band of input power by maintaining the value of input impedance for the rectifier fixed

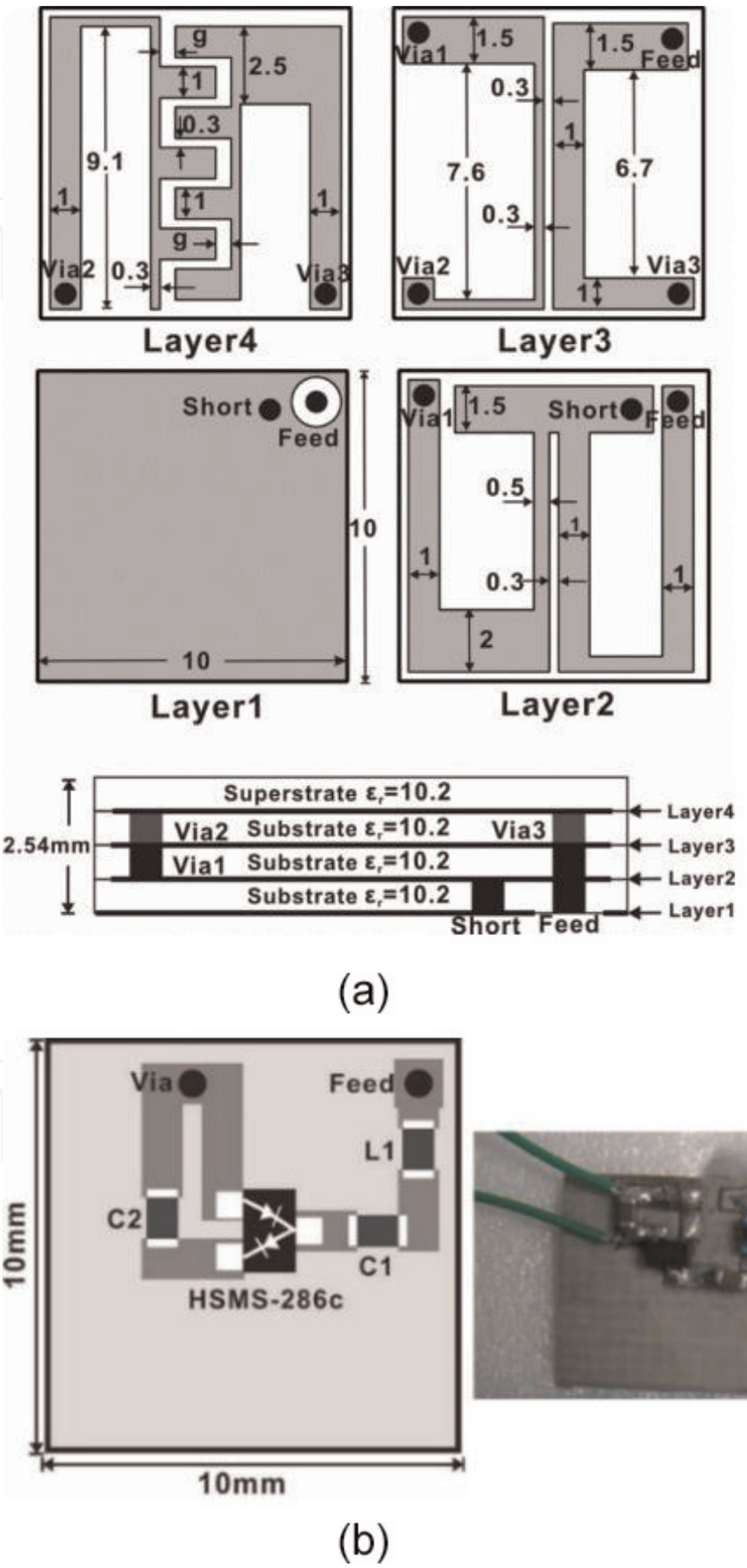

Figure 10.
(a) Triple band antenna, (b) rectifier design and a photo of a fabricated rectifier [40].

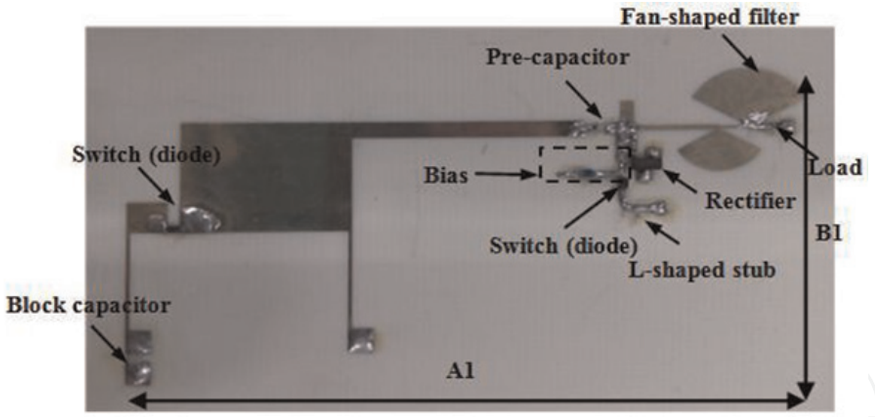

Figure 11.
Fabricated reconfigurable rectenna [41].

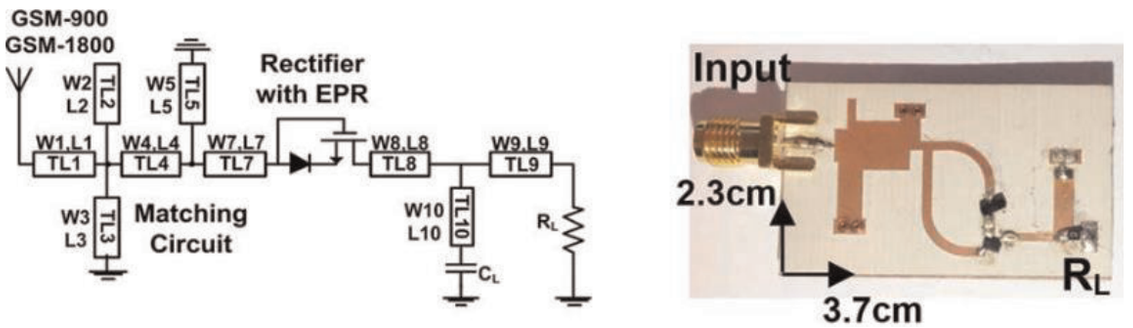

Figure 12.
Schematic diagram and fabricated circuit [43].

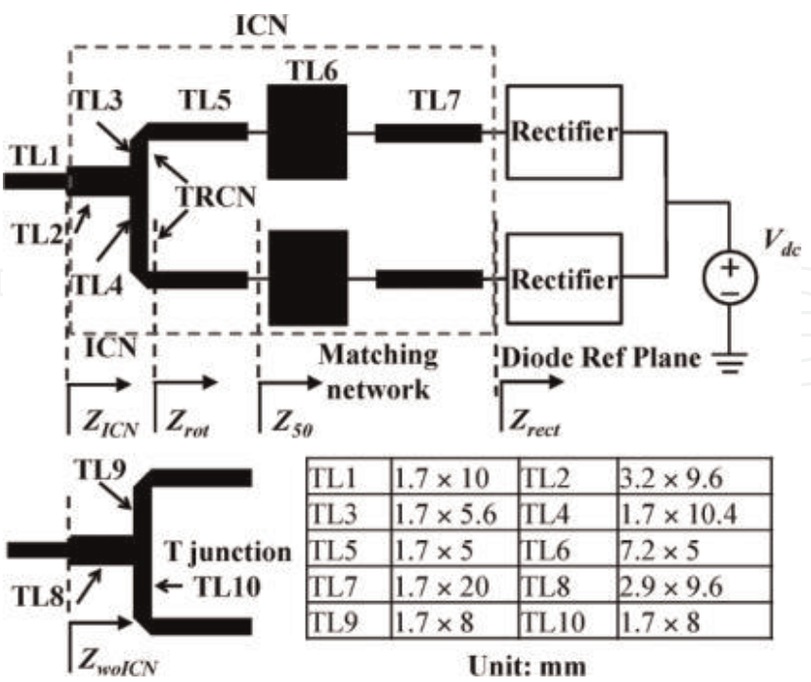

TL1	1.7 × 10	TL2	3.2 × 9.6
TL3	1.7 × 5.6	TL4	1.7 × 10.4
TL5	1.7 × 5	TL6	7.2 × 5
TL7	1.7 × 20	TL8	2.9 × 9.6
TL9	1.7 × 8	TL10	1.7 × 8

Unit: mm

Figure 13.
Layout of the rectifier [44].

regardless the value of the input power. **Figure 13** shows the rectifier configuration. The rectifier has a maximum conversion efficiency of 56% at 31.8 dBm and the input power range for efficiency over than 50% is 6.7 dBm.

3. Dual-band Rectenna using voltage doubler rectifier and four-section matching network

This section introduces a dual-band rectenna with maximum measured conversion efficiency of 63 and 69% at f_1 = 1.95 and f_2 = 2.5 GHz, respectively, over wide band of the input power, 14 and 15.5 dBm for conversion efficiency above 50% at f_1 and f_2, respectively. The section arrangements are as follows: in Section 3.1, the antenna design is introduced. Then, the equivalent circuit of the antenna is discussed in Section 3.2. Antenna results (reflection coefficient as well as radiation characteristics) is discussed in Section 3.3. The rectifier-antenna matching network for the dual band is described in Section 3.4. The rectifier structure with the geometrical parameters is illustrated in Section 3.5. The rectenna experiment setup is revealed in Section 3.6. While, the rectenna performance including RF-DC conversion efficiency in addition to the DC output voltage at the two frequency bands is discussed in Section 3.7.

3.1 Antenna design

In this section, the enhanced-gain antenna design [45] is introduced to be used to configure the rectenna system. **Figure 14** shows the layout of the proposed antenna. As shown in the figure, the antenna includes two substrate layers (substrates 1 and 2). The two layers have the same substrate material with relative dielectric constant $\varepsilon_{r1} = \varepsilon_{r2} = 3.55$, thickness h_1 = h_2 = 0.813 mm and a loss tangent of 0.0027. The antenna design consists of disc antenna printed on the top layer of substrate 1. The resonance frequency of this disc is inversely proportional to the disc radius as shown in Eq. (1) [46] which can be determined from Eq. (2) [46]. This disc is directly fed by a microstrip line with 50Ω through a via with radius of 0.6 mm. Also, this disc feeds (by coupling) a circular slot on the ground plane between the feed line and the radiating patch, a square reflecting plane with defected reflector structure (DRS) placed behind the antenna at a distance of $\lambda_0/8$ to improve the antenna gain as well as enhance the front to back ratio. The reflector is built on 0.8 mm thick FR4 substrate with dielectric constant of 4.4 and a loss tangent of 0.02. The reflector is supported by a 15 mm thick layer of lightweight

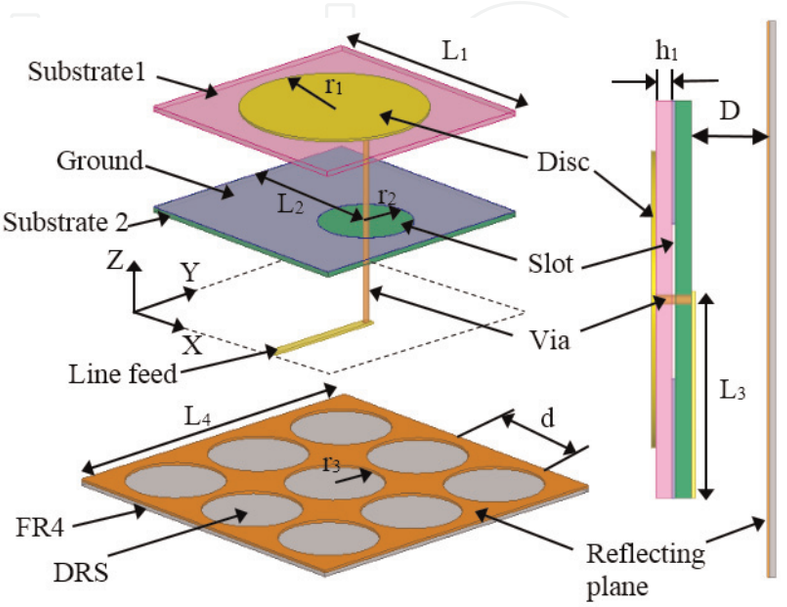

Figure 14.
3D geometry, perspective view and side view of the proposed disc antenna [45].

foam with a low dielectric constant ($\varepsilon_r = 1.06$). Substrate dimensions are 50 mm × 50 mm. The designated antenna resembles good candidate for RF energy harvesting from mobile radio waves (f_1 = 1.95 GHz) and from WLAN wireless communication systems (f_2 = 2.45 GHz).

$$f_r = \frac{1.8412 v_0}{2\pi a_e \sqrt{\varepsilon_r}} \tag{1}$$

$$a_e = a\left[1 + \frac{2h}{\pi a \varepsilon_r}\left(\ln\left(\frac{\pi a}{2h}\right) + 1.7726\right)\right]^{0.5} \tag{2}$$

3.2 Equivalent circuit of the proposed antenna (modeling of patch antenna)

The first challenge of designing the equivalent circuit was to find an accurate model of the proposed antenna at f_1 and f_2. **Figure 15** shows the equivalent circuit used to model the electrical behavior of the antenna in response to an incoming RF input signal. It is useful to implement this model using basic components R1, L1, and C1, which represent the influence of the first resonant frequency (f_1), whereas R2, L2, and C2 represent the second resonant frequency (f_2). Elements L3 and C3 are included in the equivalent circuit model to represent the electrical length of the feed line and slot coupling, respectively. The resistance R1 and R2 correspond to radiating losses.

Each radiator (the disc and the slot) is represented by a resonator. Each resonator consists of parallel RLC circuit, the resonance frequency of each one can be determined from Eq. (3):

$$f_r = \frac{1}{2\pi\sqrt{LC}} \tag{3}$$

Firstly, each resonator is studied separately. S-parameters are calculated from Agilent ADS simulator. Then the resonant and cutoff frequencies (f_0 and f_c in GHz, respectively) are determined. The initial values of L and C for each one can be calculated from Eqs. (4) and (5) [47, 48].

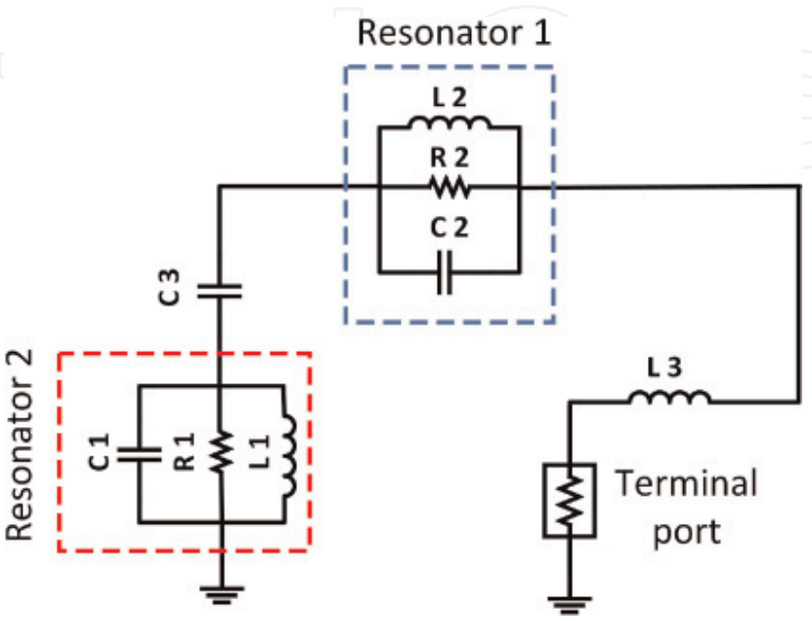

Figure 15.
Equivalent lumped-elements circuit for antenna in ADS.

$$C_p = \frac{5f_c}{\pi\left[f_0^{\,2} - f_c^{\,2}\right]}\ pF \tag{4}$$

$$L_p = \frac{250}{C_p\left[\pi f_0\right]^2}\ nH \tag{5}$$

where C_p is the capacitance in picofarads and L_p is the inductance in nanohenrys. **Table 1** summarizes the initial values of R and L at the two operating frequencies.

The losses resistance can be determined from the quality factor (Q)-frequency bandwidth relationship (BW) as:

$$Q = \frac{\omega_0}{BW} = \omega_0 RC \tag{6}$$

f_0 and f_c	C→ $\left(C_p = \frac{5f_c}{\pi\left[f_0^{\,2} - f_c^{\,2}\right]}\ pF\right)$	L → $\left(L_p = \frac{250}{C_p\left[\pi f_0\right]^2}\ nH\right)$
Resonator 1 (f_0 = 2.45 GHz & f_c = 2.25 GHz)	At f_c = 2.25 GHz and f_0 = 2.45 GHz, then: Cp = 3.8 pF	At f_0 = 2.45 GHz and Cp = 3.8 pF, then: Lp = 1.11 nH
Resonator 2 (f_0 = 1.95 GHz & f_c = 1.65 GHz)	At f_c = 1.65 GHz and f_0 = 1.95 GHz, then: Cp = 2.4 pF	At f_0 = 1.95 GHz and Cp = 2.4 pF, then: Lp = 2.8 nH

Table 1.
Initial values of L and C for the two resonators.

Parameter	R1(Ω)	L1(nH)	C1(pF)	R2(Ω)	L2(nH)	C2(pF)	L3(nH)	C3(pF)
Value	750	10	1.7	500	1.39	4.15	10	0.2

Table 2.
Elements values of the equivalent circuit model for the dual band antenna.

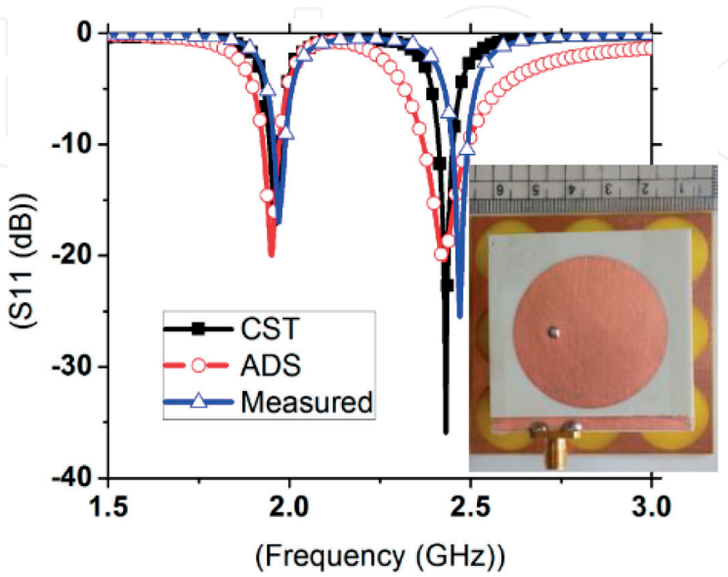

Figure 16.
Reflection coefficient of the proposed antenna.

where the half power frequency bandwidth is evaluated from Eq. (7).

$$BW = \frac{1}{RC} \tag{7}$$

Then, the loss resistance (R) for each resonator can be determined as:

$$R = \frac{1}{BW \times C} \tag{8}$$

After combining the two resonators, taking into account the effect of losses resistances (R1 and R2) in addition to making optimization, the final equivalent circuit can be obtained. The corresponding values of the equivalent circuit elements are depicted in **Table 2**.

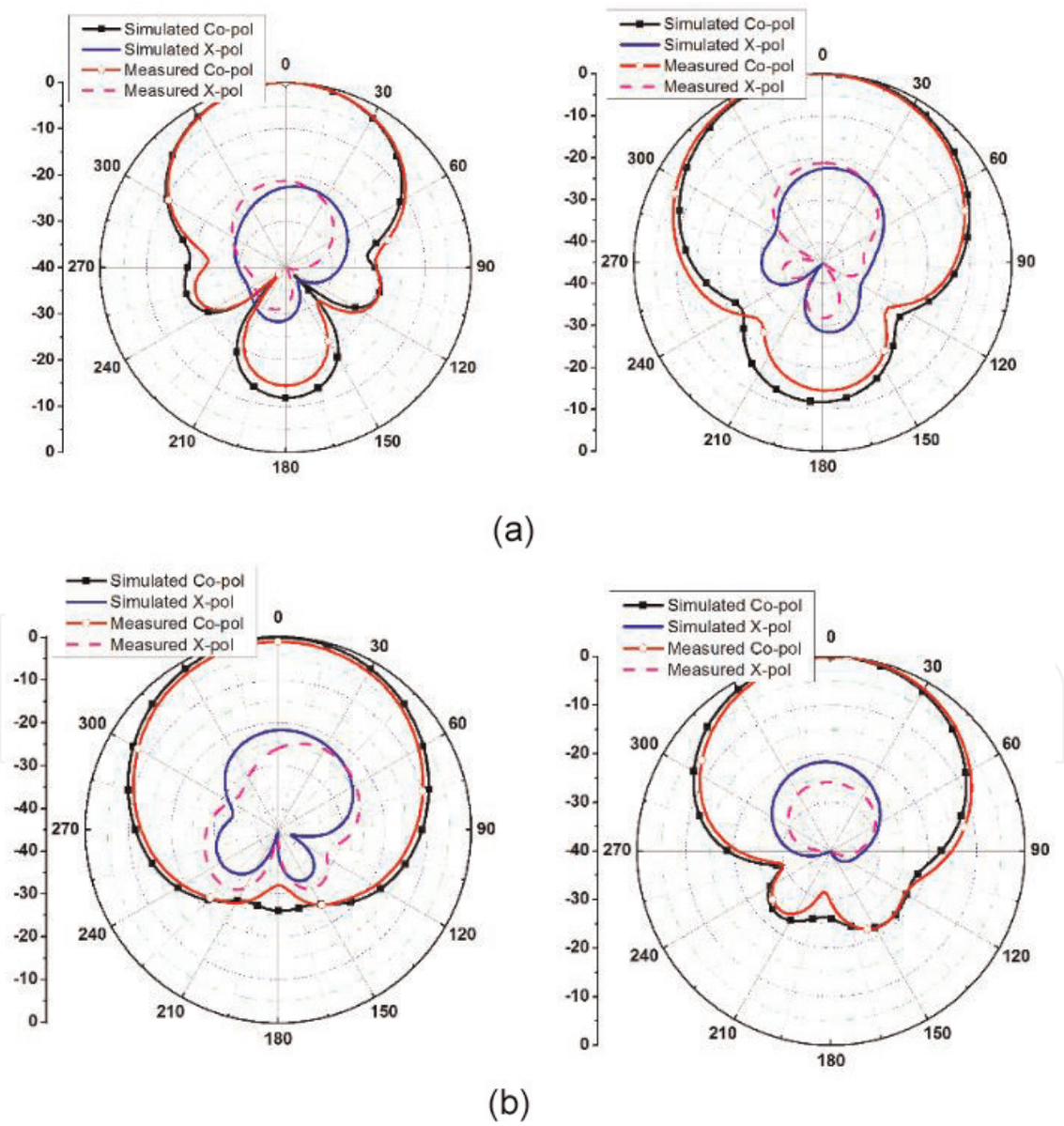

Figure 17.
2D measured and simulated results of radiation pattern for the antenna: (a) at 1.95 GHz and (b) at 2.45 GHz.

3.3 Antenna measurement results

3.3.1 Designed antenna S-parameters

Figure 16 shows the reflection coefficient response of the antenna obtained from CST simulation compared with the calculated response of the equivalent circuit model by using Agilent ADS software in addition to the measured reflection coefficient. Good agreement was between the results of simulated, measured and ADS model. The antenna resonates at two bands 1.95 GHz (f_1) and 2.45 GHz (f_2). The circular patch is designed to radiate at 2.45 GHz by the direct feed with the transmission line placed behind substrate 2. Whereas, 1.95 GHz resonance frequency is designed to radiate due to the capacitive coupling between the circular patch on the top of substrate 1 and the circular slot located on the ground plane, where in 1.95 GHz case the disc antenna is considered as a feeder for the circular slot. The performance of the proposed antenna was simulated and optimized by commercial EM software CST Microwave Studio. A prototype of the proposed antenna was fabricated and tested. The reflection coefficient of the antenna was measured by R&S ZVA 67 Network Analyzer. It is noted that the simulated and measured results of the input impedances of the antenna are in good agreement. Only, a small shift in the measured S-parameters was observed due to the connector soldering, fabrication tolerance, the adhesive between the two layers of the antenna and the layers alignment in fabrication process.

3.3.2 Radiation characteristics

The simulated and measured results of E-plane and H-plane for the high gain antenna at f_1 and f_2 are shown in **Figure 17(a)** and **(b)**, respectively. The measured values of gain, radiation efficiency, F/B ratio, cross polarization level, 3 dB angular beamwidth at the first resonance frequency (f_1) are 8.3 dBi, 90%, 12, −22.3 dB, 73.5°, respectively. While at the second resonance frequency, these values can be summarized as 7.8 dBi, 91.6%, 26, −21.6 dB, 79.5°, respectively. The gain and radiation pattern of the antenna were measured by the Anechoic Chamber shown in

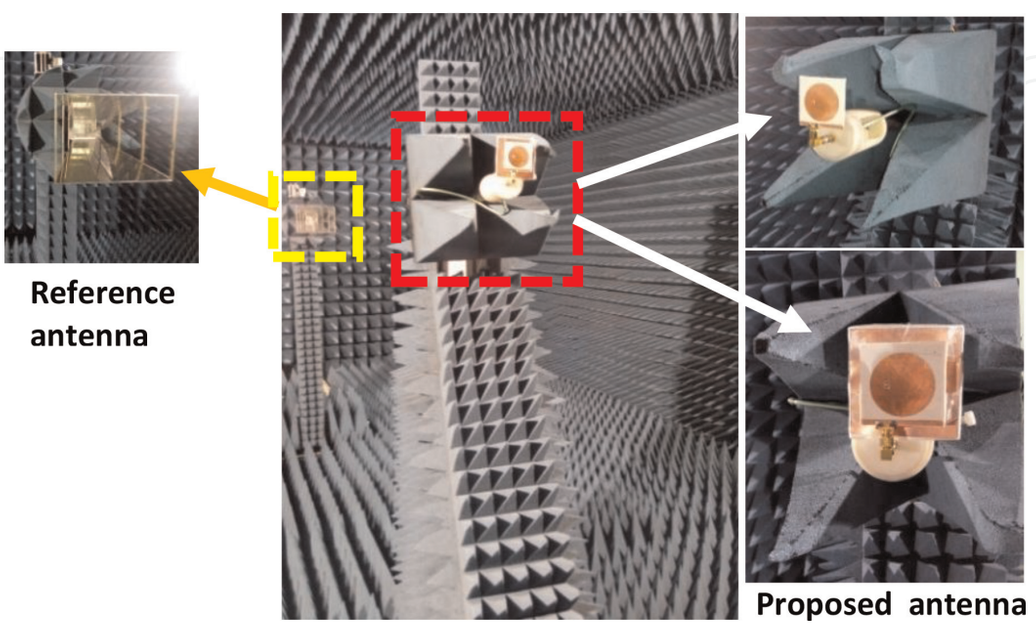

Figure 18.
Antenna radiation pattern measurement set-up.

Figure 18. There is a good agreement between the simulated and measured results of the radiation characteristics.

3.4 Rectifier-antenna matching

In this design, a scheme used in [49] is employed to achieve a dual-band impedance transformation at the two frequency bands (f_1 and f_2). This scheme is used to match between a complex and frequency-dependent rectifier input impedance (Z_{Rec}) and a real impedance of the antenna (Z_{Ant}) by using four different sections (Section 1–4) as shown in **Figure 19**. The matching technique can be summarized in the following steps:

Step 1: Achieve the conjugate matching between the load values at both resonant frequencies, that is, moving the two impedance values of the load (rectifier) on the Smith chart to be located on the same real circle with the imaginary parts are equal on both sides of the Smith chart as shown in **Figure 20**.

Step 2: Cancel the imaginary part of the impedances at f_1 and f_2.

Step 3: Real to real impedance transformation.

Each section is characterized by two values Z and θ, where Z is the section characteristic impedance and θ is the section electrical length. The function of the first section (Section 1) is to make the real value of the rectifier input impedance at

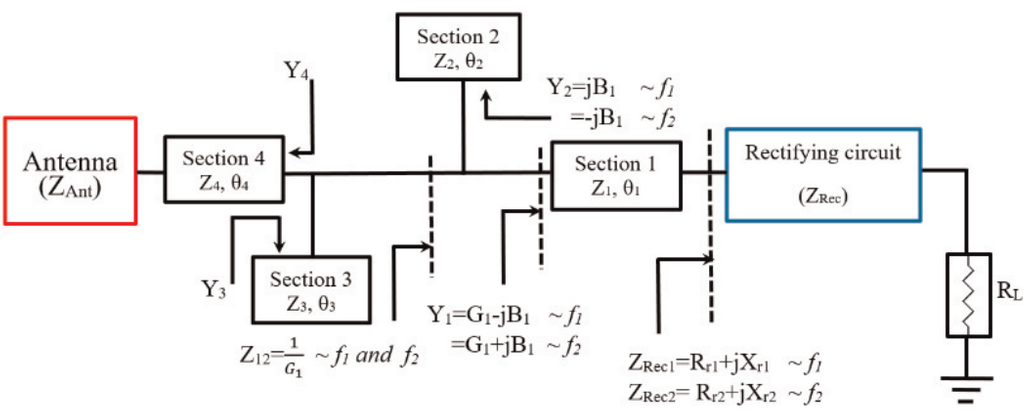

Figure 19.
Dual-band matching circuit.

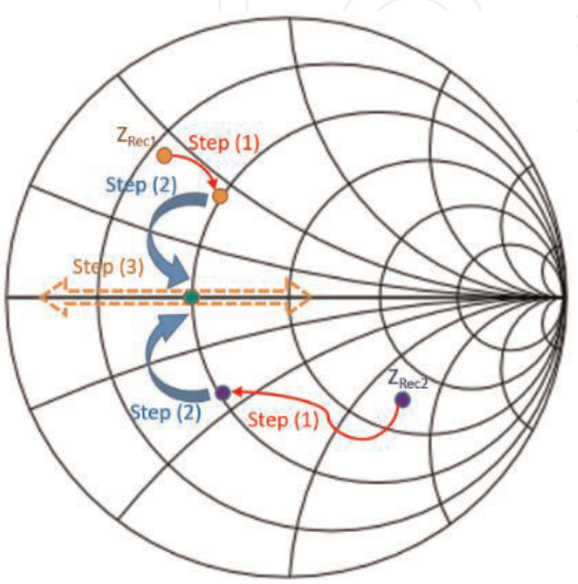

Figure 20.
Matching steps indicated on smith chart.

f_1 is equal to that of the rectifier input impedance at f_2 and the imaginary parts are also equal but with opposite signs (one is positive (inductive reactance) and the other one is negative (capacitive reactance)); Section 1 parameters (Z_1 and θ_1) can be calculated from [50] as:

$$Z_1 = \sqrt{\left(R_{r1}R_{r2} + X_{r1}X_{r2} + \frac{X_{r1} + X_{r2}}{R_{r2} - R_{r1}}\left(R_{r1}X_{r2} - R_{r2}X_{r1}\right)\right)} \tag{9}$$

$$\theta_1 = \frac{n\pi + arctan\,\frac{Z_1(R_{r1} - R_{r2})}{R_{r1}X_{r2} - R_{r2}X_{r1}}}{(m+1)} \tag{10}$$

where n is an arbitrary integer and m = f2/f1. Section 2 is used to cancel the imaginary parts of the admittance Y_1 at the two frequencies f_1 and f_2. Section 2 parameters can be determined as [49]:

$$Z_2 = \frac{\tan\theta_2}{B_1} \tag{11}$$

$$\theta_2 = \frac{(1+p)\pi}{(1+m)} \tag{12}$$

where p is an integer. Sections 3 and 4 are used for real to real impedance transformation, and their parameters can be calculated from Eqs. (13)–(17) [49, 51]

$$Z_4 = \sqrt{\left(\frac{Z_{Ant}(1 + \tan^2\theta_4)}{G_1} - Z_{Ant}^2\right)\frac{1}{\tan\,\theta_4}} \tag{13}$$

$$\theta_4 = \frac{(1+s)\pi}{(1+m)} \tag{14}$$

$$Z_3 = \frac{\tan\theta_3}{B_4} \tag{15}$$

$$\theta_3 = \frac{(1+q)\pi}{(1+m)} \tag{16}$$

$$B_4 = \frac{\left(Z_{Ant}^2 - Z_4^2\right)\tan\theta_4}{Z_{Ant}^2 \times Z_4 + Z_4^3 \times \tan^2\theta_4} \tag{17}$$

where q and s are integers.

3.5 Rectifier design

Several rectifiers' topologies are used for energy harvesting, for instance, diodes in parallel connection, diodes in series connection, voltage doubler circuits, multi-stage voltage multiplier and so forth. Voltage multipliers generate high voltages from a low voltage power source. However, in this design a half-wave voltage doubler circuit, which is a special case of voltage multipliers, is used for the rectification to get high voltage with conservation of the design simplicity. The rectifier design as well as the matching network is depicted in **Figure 21** [52]. The voltage doubler circuit comprises two Avago HSMS2850 Schottky diodes and two SMD capacitors (C_s = C_p = 100 pF). The Schottky diode has a built-in voltage (V_b) of 0.150 V and a breakdown voltage (V_{br}) of 3.8 V. Due to the small values of the series resistance and the barrier capacitance (R_s of 25Ω and C_b of 0.18 pF) for the

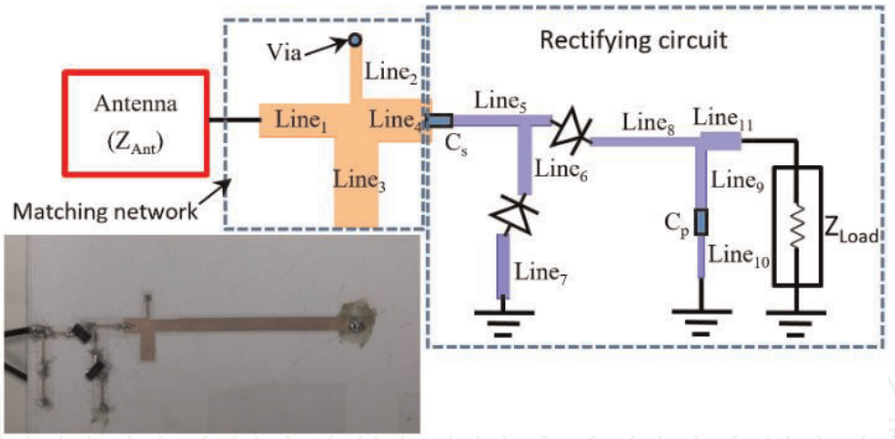

Figure 21.
Rectifier layout; L_1 = 4.5 mm, W_1 = 1.54 mm, L_2 = 4 mm, W_2 = 0.33 mm, L_3 = 5 mm, W_3 = 1.96 mm, L_4 = 3.52 mm, W_4 = 2 mm, L_5 = 4 mm, W_5 = 0.36 mm, L_6 = 4.98 mm, W_6 = 0.31 mm, L_7 = 5 mm, W_7 = 0.29 mm, L_8 = 5.1 mm, W_8 = 0.43 mm, L_9 = 4.8 mm, W_9 = 0.3 mm, L_{10} = 4.88 mm, W_{10} = 0.33 mm, L_{11} = 1.81 mm, W_{11} = 0.84 mm.

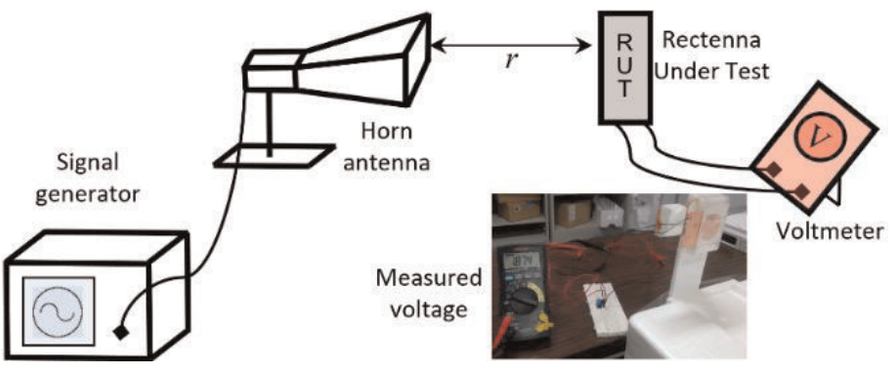

Figure 22.
Rectenna measurement setup.

above-mentioned diodes category, so these diodes have a high cutoff frequency and high conversion efficiency. The capacitor C_s is used to store the energy in one half cycle to double the charging voltage for C_p at the other half cycle, C_s also acts as bandpass filter to block the DC voltage generated from the nonlinear diodes. C_p has two functions, it is used for bypassing the higher order modes, generated from the nonlinear diode to the ground and getting a smooth DC output voltage as well. Also the shunt connection between C_p and the load impedance R_L acts as a low pass filter.

The rectifier is designed on Rogers Duroid RO3003 with a relative permittivity (ε_r) of 3, substrate thickness (h) of 0.76 mm, a dielectric loss tangent (tanδ) of 0.0013 and a copper thickness (t) of 0.017 mm. The simulated complex rectifier input impedance (Z_{Rec}) at two frequencies are (8 $-$j $\times$ 28.2) and (26.1 $-$j $\times$ 39.7) at f_1 and f_2, respectively, with a resistive load of 1.5 kΩ. The circuit parameters have been optimized to achieve the maximum conversion efficiency at the two frequency bands for the received input power levels. The parameters of the rectifier as well as the matching circuit are illustrated in **Figure 21**, where each line is defined by the length (L) and width (W). Also, the prototype of the fabricated rectifier is shown in **Figure 21**.

3.6 Rectenna measurements

The rectifying circuit including the matching network is simulated using Keysight advanced design system (ADS), while the antenna was designed using

ANSYS high-frequency structure simulator (HFSS). The enhanced-gain antenna described in [45] is used as a receiving antenna in the proposed rectenna to increase the rectifier sensitivity. Hence, increasing rectenna capability to harvest from low input power levels. The receiving antenna and the rectifier are integrated on the same substrate, fabricated and measured in the measurement setup shown in **Figure 22**. An Agilent Technologies E8257D Analog signal generator is used to send a microwave signal which is connected to a horn antenna with 9 dBi gain at the two frequencies. On the other hand, the rectenna under test (RUT) is connected with a voltmeter to measure the DC output voltage. To take the antenna radiation characteristics into account, the antenna effective area is considered. Hence, the RF-DC conversion efficiency of the proposed rectenna (η) is calculated as the following:

$$\eta = \frac{V_{DC}^2}{P_{in} \times R_L} \times 100 \tag{18}$$

where V_{DC} is the measured DC output voltage, Pin is the received RF input power and R_L is the resistive load. P_{in} is defined in Eq. (19)

$$P_{in} = P_D \times A_{eff} \tag{19}$$

where P_D is the RF power density and A_{eff} is the antenna effective area. P_D and A_{eff} are calculated using Eqs. (20) and (21), respectively.

$$P_D = \frac{P_t G_t}{4\pi r^2} \tag{20}$$

$$A_{eff} = G_r \frac{\lambda^2}{4\pi} \tag{21}$$

P_t is the transmitting power, G_t is the horn antenna gain and r is the distance between the transmitter and the rectenna all are known. Therefore, the RF-to-DC conversion efficiency can be measured. For far-field measurements, r is chosen of 40 cm. **Figure 23** shows the photo of the rectenna measurement setup.

3.7 Rectenna results and discussion

The entire system (antenna, matching circuit and rectifier) is tested over different input power levels with different resistive load values at two frequencies

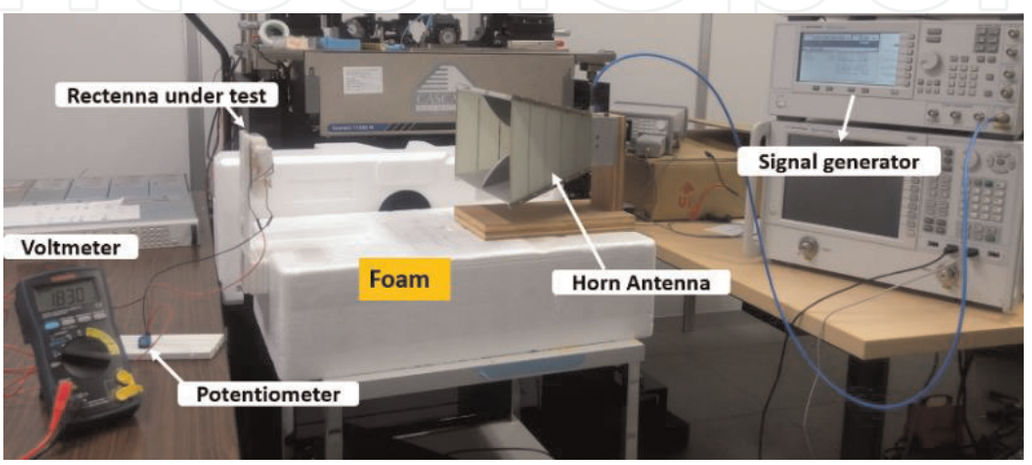

Figure 23.
Photo of the measurement setup.

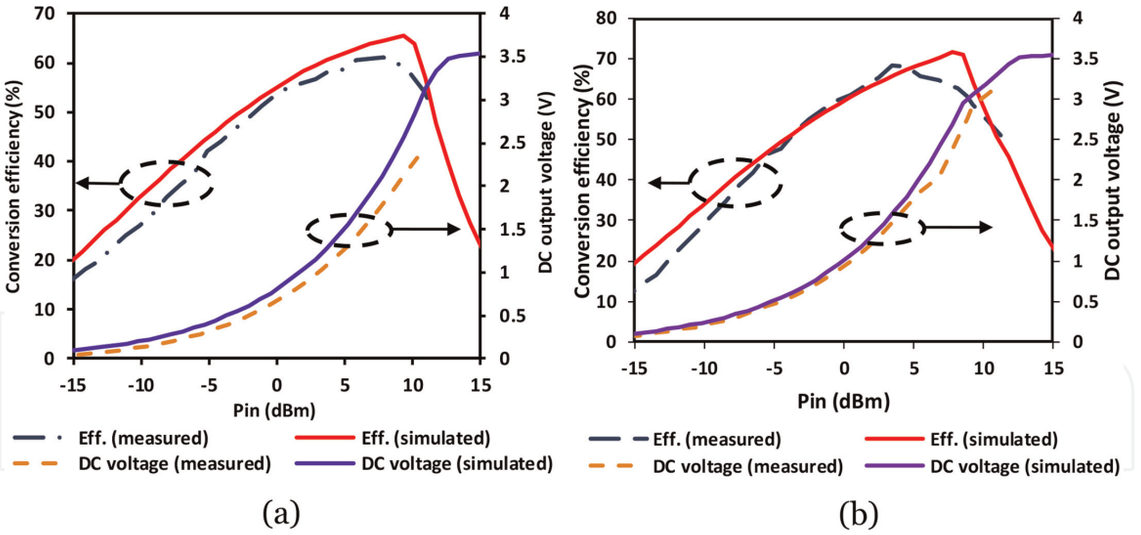

Figure 24.
Simulated and measured conversion efficiency in addition to the DC output voltage versus input power (a) at f_1 (b) at f_2.

(f_1 and f_2); **Figure 24(a)** and **(b)** show the comparison between the measured and simulated results of RF-to-DC conversion efficiency and the DC output voltage versus the input power at f_1 and f_2, respectively. The maximum measured conversion efficiency is 63% with input power range of 14 dBm (from −3.5 to 10.5 dBm) at f_1, while the measured efficiency at f_2 is 69% with input power from −4.5 to 11 dBm (15.5 dBm). There is a slight shift between the simulation and measurement results, where the maximum simulated RF-DC conversion efficiency are 66 and 73% at the same two frequencies, respectively. Due to the limitations in the experiments, the received input power is limited only up to 11 dBm.

4. Conclusions

This chapter presents a study of rectenna systems for RF energy harvesting and wireless power transfer. A survey about employing rectennas in WPT, low input received power rectennas, single and multi-band rectennas, wide input received power rectennas are introduced. Finally, dual-band rectenna using voltage doubler rectifier and four-section matching network is discussed. The first part of the rectenna design is the dual-band disc antenna with enhanced gain in order to collect a highest amount of RF energy. It radiates at 1.95 and 2.45 GHz. The measured results showed the gain of 8.3 and 7.8 dBi at 1.95 and 2.45 GHz, respectively. The disc antenna is integrated with a dual-band rectifier with four-section matching network to introduce a dual-frequency rectenna with higher conversion efficiency over wide band of the input power for multiband RF energy harvesting. The rectenna gives maximum RF-DC measured conversion efficiency of 63% and 69% at 1.95 GHz and 2.5 GHz, respectively. it also operates over a wide range of the input power; it covers the range of 14 and 15.5 dBm at f_1 and f_2, respectively for a conversion efficiency higher than 50% with load resistance (R_L) = 1K. The rectenna is simulated, fabricated and measured. The simulated and measured results show good agreement.

Author details

Mohamed Aboualalaa* and Hala Elsadek
Electronics Research Institute, Cairo, Egypt

*Address all correspondence to: mohamed.ali@ejust.edu.eg

References

[1] Kim D, Park J, Park HH, Ahn S. Generation of magnetic propulsion force and torque for microrobot using wireless power transfer coil. EEE Transactions on Magnetics. 2015;**51**(11): 1-4

[2] Ahn D, Kim S-M, Kim S-W, Moon J, Cho I-K. Wireless power transfer receiver with adjustable coil output voltage for multiple receivers application. IEEE Transactions on Industrial Electronics. 2018;**66**(5): 4003-4012

[3] Kim T, Yun G, Lee WY, Yook J. Asymmetric coil structures for highly efficient wireless power transfer systems. IEEE Transactions on Microwave Theory and Techniques. 2018;**66**(7):3443-3451

[4] Hekal S, Abdel-Rahman AB, Jia H, Allam A, Pokharel RK, Kanaya H. Strong resonant coupling for short-range wireless power transfer applications using defected ground structures. In: IEEE Wireless Power Transfer Conference (WPTC), Colorado, USA. 2015

[5] Hekal S, Abdel-Rahman AB, Jia H, Allam A, Barakat A, Pokharel RK. A novel technique for compact size wireless power transfer applications using defected ground structures. IEEE Transactions on Microwave Theory and Techniques. 2017;**65**(2):591-599

[6] Tahar F, Barakat A, Saad R, Yoshitomi K, Pokharel RK. Dual-band defected ground structures wireless power transfer system with independent external and inter-resonator coupling. IEEE Transactions on Circuits and Systems II: Express Briefs. 2017;**64**(12):1372-1376

[7] Sasaki S, Tanaka K, Maki K. Microwave power transmission technologies for solar power satellites. Proceedings of the IEEE. 2013;**101**(6): 1438-1447

[8] McSpadden P, Jaffe J. Energy conversion and transmission modules for space solar power. Proceedings of the IEEE. 2013;**101**(6):1424-1437

[9] Li X, Duan B, Song L, Zhang Y, Xu W. Study of stepped amplitude distribution taper for microwave power transmission for SSPS. IEEE Transactions on Antennas and Propagation. 2017;**65**(10):5396-5405

[10] Nguyen VT, Kang SH, Choi JH, Jung CW. Magnetic resonance wireless power transfer using three-coil system with single planar receiver for laptop applications. IEEE Transactions on Consumer Electronics. 2015;**61**(2): 160-166

[11] Low ZN, Chinga RA, Tseng R, Lin J. Design and test of a high-power high-efficiency loosely coupled planar wireless power transfer system. IEEE Transactions on Industrial Electronics. 2009;**56**(5):1801-1812

[12] Wireless Charging Pad, Black Sapphire. Samsung Mobile, Samsung Electronics America. [Online]. Available from: http://www.samsung.com/us/mobile/cell-phones-accessories/eppg920ibugus

[13] Wang G, Liu W, Sivaprakasam M, Kendir GA. Design and analysis of an adaptive transcutaneous power telemetry for biomedical implants. IEEE Transactions on Circuits and Systems I: Regular Papers. 2005;**52**(10):2109-2117

[14] Jou AY, Azadegan R, Mohammadi S. High-resistivity CMOS SOI rectenna for implantable applications. IEEE Microwave and Wireless Components Letters. 2017;**27**(9):854-856

[15] Loubet G, Takacs A, Dragomirescu D. Implementation of a battery-free wireless sensor for cyber-physical systems dedicated to structural health monitoring applications. IEEE Access. 2019;**7**:24679-24690

[16] Awais Q, Jin Y, Chattha HT, Jamil M, Qiang H, Khawaja BA. A compact rectenna system with high conversion efficiency for wireless energy harvesting. IEEE Access. 2018;**6**: 35857-35866

[17] Shen S, Chiu C-Y, Murch RD. A dual-port triple-band L-probe microstrip patch rectenna for ambient RF energy harvesting. IEEE Antennas and Wireless Propagation Letters. 2017; **16**:3071-3074

[18] Khemar A, Kacha A, Takhedmit H, Abib G. Design and experiments of a dual-band rectenna for ambient RF energy harvesting in urban environments. IET Microwaves, Antennas and Propagation. 2018;**12**(1): 49-55

[19] Valenta CR, Durgin GD. Harvesting wireless power: Survey of energy-harvester conversion efficiency in far-field, wireless power transfer systems. IEEE Microwave Magazine. 2014;**15**(4): 108-120

[20] Nie M, Yang X, Tan G, Han B. A compact 2.45-GHz broadband rectenna using grounded coplanar waveguide. IEEE Antennas and Wireless Propagation Letters. 2015;**14**:986-989

[21] Assimonis SD, Daskalakis S, Bletsas A. Sensitive and efficient RF harvesting supply for batteryless backscatter sensor networks. IEEE Transactions on Microwave Theory and Techniques. 2016;**64**(4):1327-1338

[22] Haboubi W, Takhedmit H, Luk J-DLS, Adami S-E, Allard B, Costa F, et al. An efficient dual-circularly polarized rectenna for RF energy harvesting in the 2.45 GHz ISM band. Progress In Electromagnetics Research. 2014;**148**: 31-39

[23] Chou J, Lin D, Weng K, Li H. All polarization receiving rectenna with harmonic rejection property for wireless power transmission. IEEE Transactions on Antennas and Propagation. 2014; **62**(10):5242-5249

[24] Collado A, Georgiadis A. Optimal waveforms for efficient wireless power transmission. IEEE Microwave and Wireless Components Letters. 2014; **24**(5):354-356

[25] Song C, Huang Y, Carter P, Zhou J, Joseph SD, Li G. Novel compact and broadband frequency-selectable rectennas for a wide input-power and load impedance range. IEEE Transactions on Antennas and Propagation. 2018;**66**(7):3306-3316

[26] Okba A, Takacs A, Aubert H, Charlot S, Calmon P-F. Multiband rectenna for microwave applications. Comptes Rendus Physique. 2017;**18**(2): 107-117

[27] Pham BL, Pham A. Triple bands antenna and high efficiency rectifier design for Rf energy harvesting at 900, 1900 and 2400 MHz. In: IEEE MTT-S International Microwave Symposium Digest (MTT), USA. 2013

[28] Liu J, Zhang XY. Compact triple-band rectifier for ambient RF energy harvesting application. IEEE Access. 2018;**6**:19018-19024

[29] Sarma SS, Chandravanshi S, Akhtar MJ. Triple band differential rectifier for RF energy harvesting applications. In: Asia-Pacific Microwave Conference (APMC), New Delhi. 2016

[30] Lopez-Yela A, Segovia-Vargas D. A triple-band bow-tie rectenna for RF

energy harvesting without matching network. In: IEEE Wireless Power Transfer Conference (WPTC), Taipei. 2017

[31] Chandravanshi S, Sarma SS, Akhtar MJ. Design of triple band differential rectenna for RF energy harvesting. IEEE Transactions on Antennas and Propagation. 2018;**66**(6): 2716-2726

[32] Niotaki K, Kim S, Jeong S, Collado A, Georgiadis A, Tentzeris MM. A compact dual-band rectenna using slot-loaded dual band folded dipole antenna. IEEE Antennas and Wireless Propagation Letters. 2013;**12**:1634-1637

[33] Sun H, Guo Y, He M, Zhong Z. A dual-band rectenna using broadband Yagi antenna array for ambient RF power harvesting. IEEE Antennas and Wireless Propagation Letters. 2013;**12**: 918-921

[34] Collado A, Georgiadis A. Conformal hybrid solar and electromagnetic (EM) energy harvesting rectenna. IEEE Transactions on Circuits and Systems I: Regular Papers. 2013;**60**(8):2225-2234

[35] Noghabaei SM, Radin RL, Savaria Y, Sawan M. A high-efficiency ultra-low-power CMOS rectifier for rf energy harvesting applications. In: IEEE International Symposium on Circuits and Systems (ISCAS), Florence. 2018

[36] Yadav RK, Das S, Yadava RL. Analysis and modelling of a novel compact rectenna for indoor applications. IET Communications. 2014;**8**(15):2642-2651

[37] Xie F, Yang G, Geyi W. Optimal design of an antenna array for energy harvesting. IEEE Antennas and Wireless Propagation Letters. 2013;**12**:155-158

[38] Monti G, Tarricone L, Spartano M. X-band planar rectenna. IEEE Antennas and Wireless Propagation Letters. 2011; **10**:1116-1119

[39] Mavaddat A, Armaki SHM, Erfanian AR. Millimeter-wave energy harvesting using 4×4 microstrip patch antenna array. IEEE Antennas and Wireless Propagation Letters. 2015;**14**: 515-518

[40] Huang F, Lee C, Chang C, Chen L, Yo T, Luo C. Rectenna application of miniaturized implantable antenna design for triple-band biotelemetry communication. IEEE Transactions on Antennas and Propagation. 2011;**59**(7): 2646-2653

[41] Lu P, Yang XS, Li JL, Wang BZ. A compact frequency recongurable rectenna for 5.2 and 5.8 GHz wireless power transmission. IEEE Transactions on Power Electronics. 2015;**30**(11): 6006-6010

[42] Lu P, Yang X-S, Li J-L, Wang B-Z. A dual-frequency quasi-pifa rectenna with a robust voltage doubler for 2.45 and 5.8 GHz wireless power transmission. Microwave and Optical Technology Letters. 2015;**57**(2):319-322

[43] Liu Z, Zhong Z, Guo Y. Enhanced dual-band ambient RF energy harvesting with ultra-wide power range. IEEE Microwave and Wireless Components Letters. 2015;**25**(9): 630-632

[44] Xu J, Ricketts DS. An efficient, watt-level microwave rectifier using an impedance compression network (ICN) with applications in outphasing energy recovery systems. IEEE Microwave and Wireless Components Letters. 2013; **23**(10):542-544

[45] Aboualalaa M, Abdel-Rahman AB, Allam A, Elsadek H, Pokharel RK. Design of a dual-band microstrip antenna with enhanced gain for energy harvesting applications. IEEE Antennas

and Wireless Propagation Letters. 2017; **16**:1622-1626

[46] Balanis CA. Modern Antenna Handbook. New York: John Wiley & Sons; 2011

[47] Ahn D, Park J, Kim C, Kim J, Qian Y, Itoh T. A design of the low-pass filter using the novel microstrip defected ground structure. IEEE Transactions on Microwave Theory and Techniques. 2001;**49**(1):86-93

[48] Abdel-Rahman AB, Verma AK, Boutejdar A, Omar AS. Control of bandstop response of Hi–Lo microstrip low-pass filter using slot in ground plane. IEEE Transactions on Microwave Theory and Techniques. 2004;**52**(3): 1008-1013

[49] Maktoomi MA, Gupta R, Hashmi MS. A dual-band impedance transformer for frequency-dependent complex loads incorporating an L-type network. In: Asia-Pacific Microwave Conference (APMC), Nanjing. 2015

[50] Liu X, Liu Y, Li S, Wu F, Wu Y. A three-section dual-band transformer for frequency-dependent complex load impedance. IEEE Microwave and Wireless Components Letters. 2009; **19**(10):611-613

[51] Monzon C. Analytical derivation of a two-section impedance transformer for a frequency and its first harmonic. IEEE Microwave and Wireless Components Letters. 2002;**12**(10): 381-382

[52] Aboualalaa M, Mansour I, Bedair A, Allam A, Zahhad MA, Elsadek H, et al. Dual-band rectenna using voltage doubler rectifier and four-section matching network. In: IEEE Wireless Power Transfer Conference (WPTC), Montreal, QC, Canada. 2018